Journal of Physics: Condensed Matter

PAPER

Anisotropic superconducting property studies of single crystal $PbTaSe_2$

To cite this article: Raman Sankar *et al* 2017 *J. Phys.: Condens. Matter* **29** 095601

IOP Publishing Journal of Physics: Condensed Matter

J. Phys.: Condens. Matter **29** (2017) 095601 (7pp) doi:10.1088/1361-648X/aa4edb

Anisotropic superconducting property studies of single crystal $PbTaSe_2$

Raman Sankar[1,2], **G Narsinga Rao**[1,3], **I Panneer Muthuselvam**[1,2],
Tay-Rong Chang[4], **H T Jeng**[4], **G Senthil Murugan**[2], **Wei-Li Lee**[1] and
F C Chou[2,5,6]

[1] Institute of Physics, Academia Sinica, Taipei 11529, Taiwan
[2] Center for Condensed Matter Sciences, National Taiwan University, Taipei 10617, Taiwan
[3] Marri Laxman Reddy Institute of Technology and Management, Dundigal, Hyderabad 500043, India
[4] Department of Physics, National Tsing Hua University, Hsinchu 30013, Taiwan
[5] National Synchrotron Radiation Research Center, Hsinchu 30076, Taiwan
[6] Taiwan Consortium of Emergent Crystalline Materials, Ministry of Science and Technology, Taipei 10622, Taiwan

E-mail: sankarndf@gmail.com and fcchou@ntu.edu.tw

Received 1 August 2016, revised 10 November 2016
Accepted for publication 21 November 2016
Published 18 January 2017

Abstract

The anisotropic superconducting properties of $PbTaSe_2$ single crystal is reported. Superconductivity with $T_c = 3.83 \pm 0.02$ K has been characterized fully with electrical resistivity $\rho(T)$, magnetic susceptibility $\chi(T)$, and specific heat $C_p(T)$ measurements using single crystal samples. The superconductivity is type-II with lower critical field H_{c1} and upper critical field H_{c2} of 65 and 450 Oe ($H\perp$ to the *ab*-plane), 140 and 1500 Oe ($H\|$ to the *ab*-plane), respectively. These results indicate that the superconductivity of $PbTaSe_2$ is anisotropic. The superconducting anisotropy, electron–phonon coupling λ_{ep}, superconducting energy gap Δ_0, and the specific heat jump $\Delta C/\gamma T_c$ at T_c confirms that $PbTaSe_2$ can be categorized as a bulk superconductor.

Keywords: $PbTaSe_2$, superconductor, magnetic materials

(Some figures may appear in colour only in the online journal)

Introduction

The discovery of superconductivity in the non-centrosymmetric materials, such as heavy fermion $CePt_3Si$ and half-Heusler YPtBi compounds, has initiated widespread research activities in the field of unconventional superconductors [1–3]. The absence of an inversion symmetry creates an asymmetric electric field gradient, which splits the two fold spin degenerated electronic band into two non-degenerate separated bands [4, 5]. In these non-centrosymmetric superconductors (NCS), the new Cooper paring states, i.e. coexistence of even and odd parity Cooper pair states are predicted, instead of the conventional type of Cooper pairing in either spin-singlet or spin-triplet [4]. The NCS superconductors have been identified in different materials groups, including heavy fermion, compounds with long range magnetic ordering, such as $CePt_3Si$, $CeRhSi_3$ and UIr [1–3, 6–8], metallic compounds of strong electronic correlation [9], and weakly correlated materials like Mo_3Al_2C and $Li_2(Pd_{1-x}Pt_x)_3B$ [10–12].

Recently, Ali *et al* reported the existence of superconductivity in a non-centrosymmetric polycrystalline $PbTaSe_2$ sample, which is derived from the typical transition metal dichalcogenide $TaSe_2$ with Pb atoms intercalated between the original van der Waals gap [13]. A comparative study between the single crystal and polycrystalline forms is desirable to learn more about the expected anisotropic physical properties of the layered compound using single crystal samples.

In this article, we report the successful growth of $PbTaSe_2$ single crystal sample using a chemical vapor transport (CVT) technique. Magnetic susceptibility, transport and specific heat measurement results clearly indicate that single crystal $PbTaSe_2$ is superconducting with a superconducting transition

1361-648X/17/095601+7$33.00

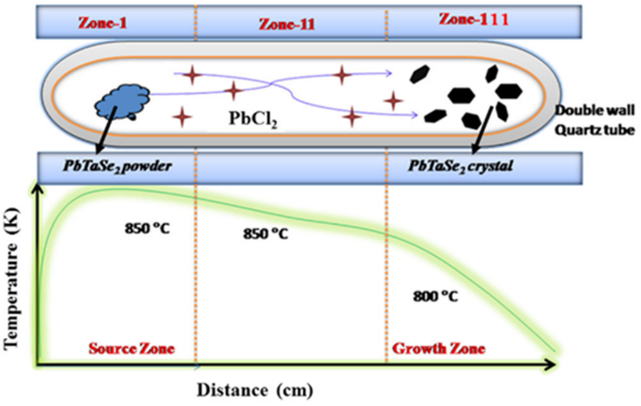

Figure 1. Cross-sectional side view of a double wall quartz tube sitting in a 3-zone tube furnace used for chemical vapor transport growth of PbTaSe$_2$ single crystals. The growth profile is shown below with set temperatures described in the text.

temperature of $T_c \sim 3.8$ K. The higher value of upper critical field $H_{c2}(0)$ is found with anisotropy compared to the reported polycrystalline sample [13].

Expermental details

Chemical vapor transport method was employed with PbCl$_2$ as the transport agent for the PbTaSe$_2$ crystal growth, which allows an effective and faster vapor transport to produce the necessary super saturation of the expected final product. Stoichiometric amount of Pb:Ta:Se (6 N purity for Pb and Ta and 5 N for Se) was loaded into a quartz ampoule, evacuated, sealed and fed into a furnace (850 °C) for 5 days. About 10 g of the pre-reacted PbTaSe$_2$ powder was placed together with a variable amount of PbCl$_2$ (purity 5 N) (50–75 mg) at one end of the silica ampoule (length 30–35 cm with inner diameter of 2.0 cm and outer diameter of 2.5 mm). All treatments were carried out in a glove box, with continuous purification of the Argon gas of oxygen and water level kept below 1 ppm. The loaded ampoule was evacuated, sealed and fed into a furnace for the growth next. The end of the ampoule containing the pre reacted material was held at 850 °C, while the crystals grew at the other end of the ampoule was maintained at a temperature of 800 °C (i.e. a temperature gradient near 2.5 °C cm^{-1}) for about one week. The schematic growth profile is shown in figure 1. Shiny single crystals of sizes up to $7 \times 5 \times 2$ mm^3 were obtained. The growth habit of the crystals was characterized by the dominance of (0 0 *l*) faces, as confirmed by the Laue picture and XRD with preferred, as shown in the inset of figure 2. Chlorine concentrations in the range of 2.6–3.7 mg PbCl$_2$ cm^{-3} yielded sufficiently high transport rates of 40–50 mg day^{-1}. Debye–Scherrer measurements of the lattice constants *a* and *c* at room temperature for samples taken from the pre-reacted polycrystalline PbTaSe$_2$ ($a = 3.448(3)$ Å, $c = 9.352(1)$ Å) as well as from the grown single crystals ($a = 3.4474(2)$ Å, $c = 9.3528(3)$ Å) showed good agreement with the literature values [14]. The field cooled (FC) and zero field cooled (ZFC) magnetization curves were measured in a commercial vibrating sample magnetometer (VSM, Quantum Design, USA) from 1.8 K to 7 K in the presence of various applied magnetic fields. The isothermal magnetization (*M*) data were also recorded at selected temperatures. The heat-capacity (C_p) measurements were carried out by a relaxation method using the physical properties measurement system (PPMS, Quantum Design, USA).

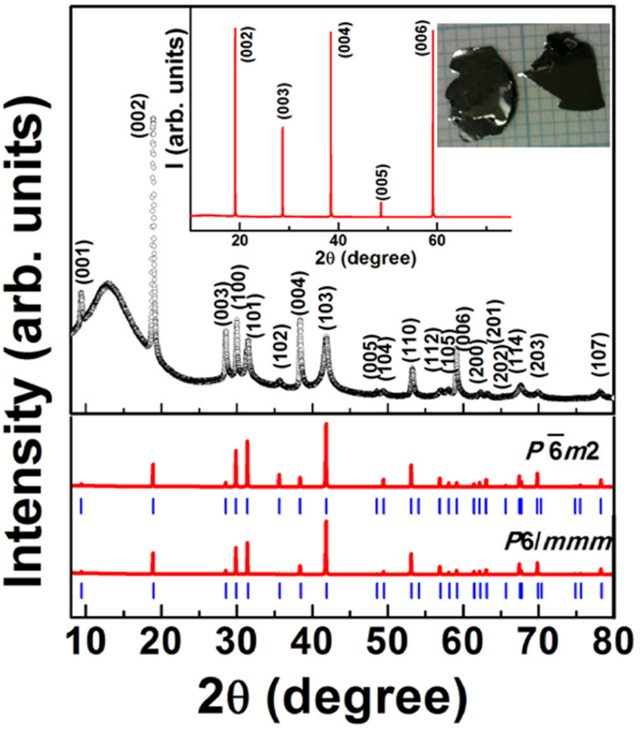

Figure 2. The powder x-ray diffraction (XRD) pattern of the as-grown sample. Simulated patterns for $P\bar{6}m2$ and $P6/mmm$ space groups are shown below with Bragg peak position marked in blue vertical bars. It is inconclusive to determine the space group from the systematic absences, however, the relatively stronger (1 0 2) peak suggests a better fitting for $P\bar{6}m2$. The crystal photo and XRD pattern for its surface with preferred orientation (0 0 *l*) are shown in the inset.

Result and discussion

Crystal structure

Figure 2(a) shows the powder x-ray diffraction (XRD) pattern and Rietveld refinement result of the pulverized as-grown PbTaSe$_2$ single crystals. All diffraction peaks can be indexed with a space group of $P\bar{6}m2$ (no. 187) or $P6/mmm$ (no. 191) equally well statistically [14]. The only difference is that the $P\bar{6}m2$ has Ta atoms order at the (1/2, 2/3, 1/2) site without centrosymmetry, and the $P6/mmm$ has a disordered distribution of Ta atoms of average half occupancy at the (1/3, 2/3, 1/2) site being centrosymmetric. The structural Rietveld refinement on the XRD pattern gives the lattice constants of $a = 3.4474$ Å and $c = 9.3528$ Å when indexed with $P\bar{6}m2$ space group, which are consistent to the reported values in the literature [14]. It is very difficult to distinguish these two space groups based on the similar systematic absences, however, the stronger (1 0 2) peak seems to suggest a better fitting to $P\bar{6}m2$. The obtained single crystals of size ~$7 \times 5 \times 2$ mm^3 can be cleaved easily to produce flat surfaces and the XRD

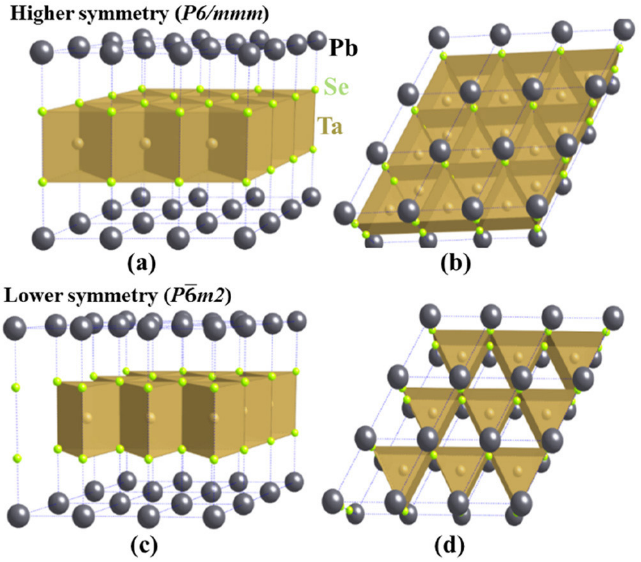

Figure 3. Crystal structures of PbTaSe$_2$ with $P6/mmm$ ((a) and (b)) and $P\bar{6}m2$ ((c) and (d)) symmetry.

pattern of the cleaved surface shows diffraction peaks with preferred orientation (0 0 l), as shown in the inset of figure 2.

While Pb:Ta = 1:1 and Ta–Se are coordinated in a trigonal prismatic coordination within each layer, the Pb atoms must sit directly in between Se atoms across layers, which leads to two possible arrangements of Ta atoms. The space group $P6/mmm$ implies that Ta atoms sit at the (1/3, 2/3, 1/2) sites of half occupancy, i.e. Ta is distributed evenly statistically without ordering within each TaSe$_2$ layer (figures 3(a) and (b)). On the other hand, the space group $P\bar{6}m2$ implies that Ta atoms sit at the (1/3, 2/3, 1/2) sites with full occupancy, i.e. the Ta is ordered within each TaSe$_2$ layer (figures 3(c) and (d)). Interestingly, the former has a centrosymmetry but the latter lacks of centrosymmetry via an spatial inversion operation of $\mathbf{r} \rightarrow -\mathbf{r}$. The stacking of the TaSe$_2$ slabs in the pristine 2H-TaSe$_2$ shows the closely packed Se atoms are 180° reversed within each unit, i.e. there are two TaSe$_2$ slabs per unit c. On the other hand, PbTaSe$_2$ has one Pb and one TaSe$_2$ trigonal prismatic slab per unit, and the Pb atoms are closely packed in parallel to the Se hexagonal close packing per layer. The stoichiometric chemical composition 1:1:2 for PbTaSe$_2$ single crystal has been confirmed by both the XRD refinement and the chemical analysis of electron probe microanalysis (EPMA) showning Pb:Ta:Se = 0.99:1:2.01 within experimental error.

Band structure

The first-principle calculations were carried out using the VASP code [15]. The energy cutoff for the plane wave expansion was 350 eV and the Brillouin zone (BZ) was sampled by a 12 × 12 × 8 and 12 × 12 × 4 mesh for the low ($P\bar{6}m2$) and high ($P6/mmm$) symmetry structures, respectively. Here we mention the high symmetry structure that be used in calculation is not $P6/mmm$, because the electronic structure code has no suitable way to handle partial occupancies. To mimic high symmetry structure, we double the unit cell along the c-direction, and shift the second layer Ta to generate inversion center. Spin–orbit coupling (SOC) was included in all calculations self-consistently.

Figure 4(a) presents the band structures of low symmetry ($P\bar{6}m2$) without inclusion of SOC. It is clearly to see that the Pb 6p and Ta 5d orbitals dominate the bands around the Fermi level (E_{F}) [16]. The Pb 6p states display the electron-like band dispersion and cross with hole-like Ta 5d states, forming a spinless nodal-line around E_{F} as shown in figure 4(c). Spinless nodal-line has been predicted in many materials such as Cu$_3$PdN [17], Cu$_3$ZnN [18] and Ca$_3$P$_2$ [19]. However, SOC is a native quantity in real materials, which is impossible to 'switch off'. In previous works, spinless nodal-lines are gapped out when SOC included, indicating these materials are not convincing candidates for study nodal-line physics in experiments. In PbTaSe$_2$ with low symmetry structure ($P\bar{6}m2$), each band around K (figure 4(e)) and H points (figure 4(f)) split into two branches when SOC was turned on (figure 4(d)). Thanks to the crystalline reflection symmetry, band crossing on the crystalline mirror plane can be remained when they carry opposite mirror reflection eigenvalues [20]. Therefore, the nodal-lines on A–H–L and Γ–K–M planes do not gaped by SOC. In PbTaSe$_2$ with low symmetry ($P\bar{6}m2$), there are one and two node-lines around K and H point, respectively, which are not only protected by the mirror reflection symmetry but also characterized by an integer topological invariant [20]. More theoretical and experimential results related node-line physics were published in [20]. Figure 4(g) shows the band structures of high symmetry ($P6/mmm$) without inclusion of SOC. At the fisrst glance, this band structure is similar to low symmety case, only minor difference due to the different size of the BZ in the z-direction. Thus the spinless nodal-line in high symmetry structure is on $k_z = 0$ plane (figure 4(h)), not on $k_z = \pi$ (figure 4(i)). When SOC was turned on, the band dispersion of high-symmetry PbTaSe$_2$ shows band splitting features which is similar to the low-symmetry case. However, all bands are spin doubly degenerate due to the crystal inversion symmetry in high-symmetry structure. We found this unusual band structures are resulted from local symmetry breaking effect which has been extensively discussed in transition metal dichalcogenide [21–23]. In our model, high-symmetry PbTaSe$_2$ can be regarded as two low-symmetry PbTaSe$_2$ with different stacking to keep crystal inversion symmetry. Thus the inversion symmetry can be broken in local structure asymmetry and inducded significant spin band splitting, but global inversion symmetry result in spin doubly degenerated band structures. It is worth to note that all nodal-line states are actually gapped for the high-symmetry ($P6/mmm$) (figures 4(j)–(l)) when SOC was included, resulting from the missing reflection symmetry. The band crossing states are gapped due to the SOC. According to previous discussion, it is clear that the growth of low symmetry ($P\bar{6}m2$) PbTaSe$_2$ is not only an important but also a critical step to study the nodal-line physic.

Superconductivity

Magnetic properties. Figure 5 shows the field-cooled (FC) and zero-field-cooled (ZFC) magnetization curves for PbTaSe$_2$ single crystal measured in an applied magnetic field of 10 Oe,

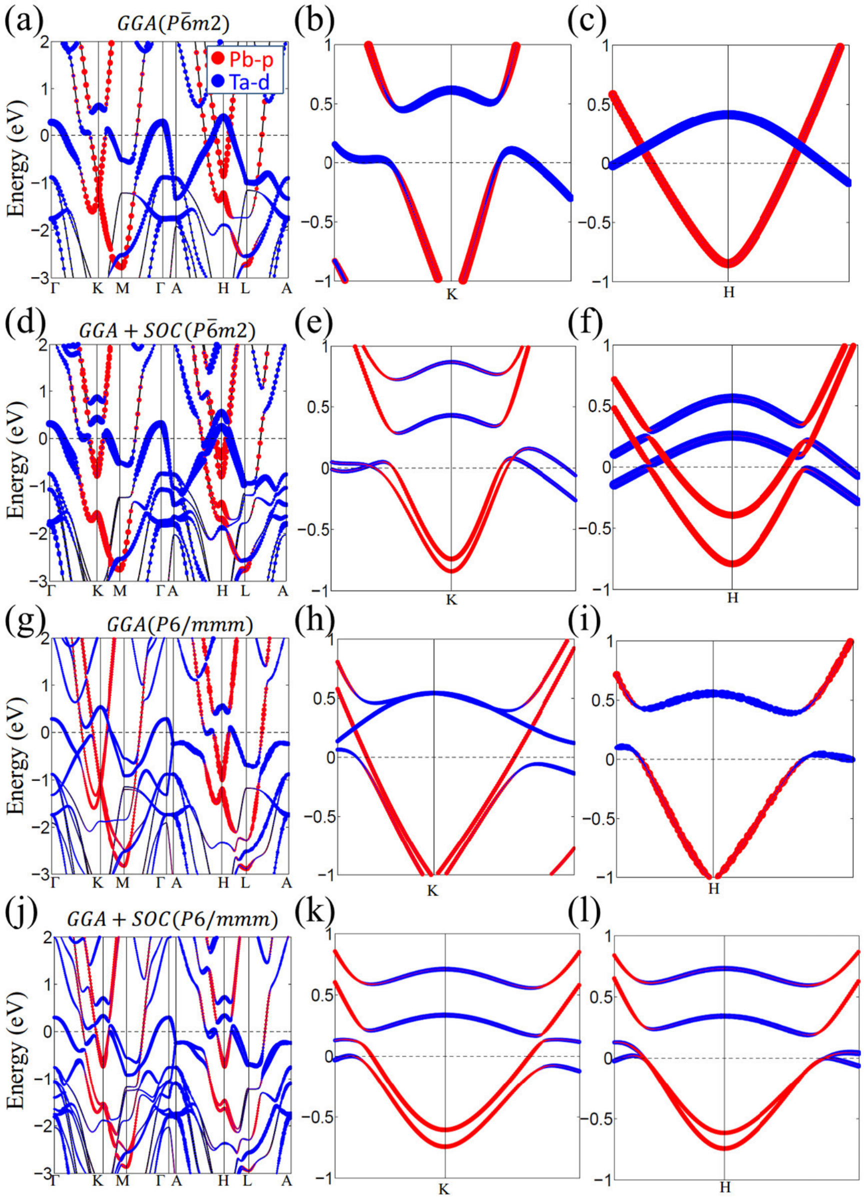

Figure 4. Band structures of PbTaSe2. (a) GGA with non-centrosymmetric ($P\bar{6}m2$) space group. (b) and (c) are the same as (a) but zoom-in band structure around K and H, respectively. (d) GGA + SOC with non-centrosymmetric ($P\bar{6}m2$). (e) and (f) are the same as (d) zoom-in band structure around K and H, respectively. (g) GGA with centrosymmetric ($P6/mmm$) space group. (h) and (i) are the same as (g) but zoom-in band structure around K and H, respectively. (g) GGA + SOC with centrosymmetric ($P6/mmm$) space group. (h) and (i) are the same as (g) but zoom-in band structure around K and H, respectively.

for both orientations of parallel (H||) and perpendicular ($H\perp$) to the *ab*-plane. The magnetic susceptibility confirms the onset of a superconducting transition temperature of T_c ~ 3.8 K, which is consistent to the recent report based on a polycrystalline sample [13]. Large diamagnetic screening is evidenced from the dimensionaless χ_{ZFC} value that approaches ~95% of the expected value of $1/4\pi$ for H perpendicular to the *ab*-plane before the geometric factor correction. Whereas a reduced diamagnetic screening is found in the dimensionless χ_{FC} value ~48% for H parallel to the *ab*-plane. The significant reduction of χ_{FC} value below T_c suggests the effect of flux pinning from defects, which is commonly observed in the superconductors with layered structure [24].

The observed strong anisotropy reflects the 2D transport network for a layered crystal structure with van der Waals gap between layers, similar to that observed in NbSe$_2$ of T_c ~ 7.2 K with a similar layered structure [25]. The isothermal magnetization $M(H)$ curves of PbTaSe$_2$ at $T = 1.8$ K for H|| and $H\perp$ to the *ab*-plane are depicted in the inset of figure 5. The hysteresis of the magnetization in the superconducting state resembles the typical behavior of a type-II superconductor. The lower critical field H_{c1}, as determined from the point of deviation from the linear M versus H of the DC magnetization data was calculated to be ~65 Oe for $H\perp$ and ~140 Oe for H|| to the *ab*-plane as shown in the inset of figure 5. The upper critical fields H_{c2} is determined from the field at the

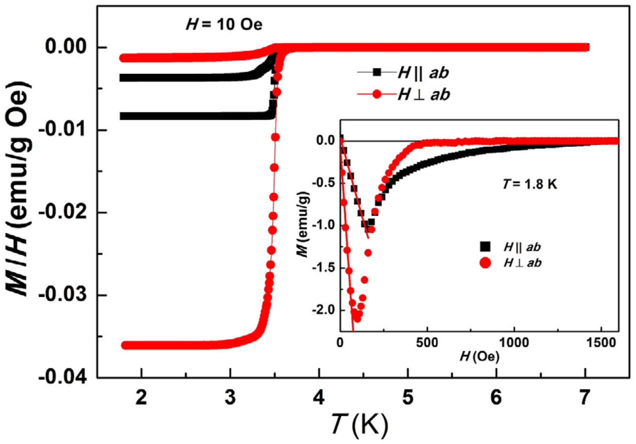

Figure 5. Zero-field cooled and field cooled dc-magnetization at $H = 10$ Oe measured for both $H \parallel$ and $H\perp$ to the *ab*-plane as a function of temperature. Inset shows the isothermal magnetization measured at 1.8 K for both $H \parallel$ and $H\perp$. The solid lines are linear fits to the data to extract H_{c1}.

intersection between the superconducting and normal states in $M(H)$. The H_{c2} values for $H \parallel$ and $H\perp$ to the *ab*-plane are found to be ~1500 Oe and ~450 Oe for at $T = 1.8$ K, respectively. The lower critical field anisotropy ratio ($H \parallel / H\perp$) is ~2, but higher for H_{c2} to be near ~3.3.

Transport properties. We have measured electrical resistivity $\rho(T)$ along different crystallographic axes (ρ_x with $I \parallel$ and ρ_z with $I\perp$ to the *ab*-plane) of a single crystal sample in zero field and in applied magnetic field along $H\perp$ to the *ab*-plane. Strong dependence on both T and H were found for the out-of-plane resistivity anisotropy, $A\perp = \rho_z/\rho_x$. The in-plane $\rho_x(I\perp H)$ and out-of-plane $\rho_z(I \parallel H)$ electrical resistivity $\rho(T)$ of single crystal PbTaSe$_2$ are shown in figure 6(a). A metallic behavior is inferred from the nearly linear T dependence of ρ and the sharp resistance drop below ~10 K for both crystallographic directions. The anisotropy $A\perp$ reaches the maximum of 2.2 at 300 K and decreases to 1.6 around 10 K. It is comparable to the anisotropy of similar layered structure NbSe$_2$ [25] andiron-arsenic high temperature superconductors AFe$_2$As$_2$ with alkali earth elements $A =$ Ca, Sr, and Ba [26].

The inset of figure 6(a) shows the expanded view at low temperatures for both crystallographic directions. Sharp superconducting transition to the zero resistance state of transition width ~0.3 K with an onset temperature T_c ~ 3.8 K is observed, which is in good agreement with that defined using the Meissner effect of susceptibility data shown in figure 5. The in-plane residual resistivity before entering the superconducting state is ρ_{norm} ~ 0.28 $\mu\Omega$ cm and with a residual resistivity ratio RRR $= \rho_{(300\text{K})}/\rho_{(5\text{K})}$ ~ 115, as shown in figure 6(a). A small residual resistivity together with a large RRR value confirms the high quality of the as-grown single crystal sample, in contrast to the RRR = 6 obtained using the polycrystalline sample [13]. The normal state resistivity data are described by the Bloch–Gruneisen (BG) model [27] as

$$\rho(T) = \rho_0 + A\left(\frac{T}{\theta_R}\right)^5 \int_0^{\frac{\theta_R}{T}} \frac{x^5 \mathrm{d}x}{(\mathrm{e}^x - 1)(1 - \mathrm{e}^{-x})} \tag{1}$$

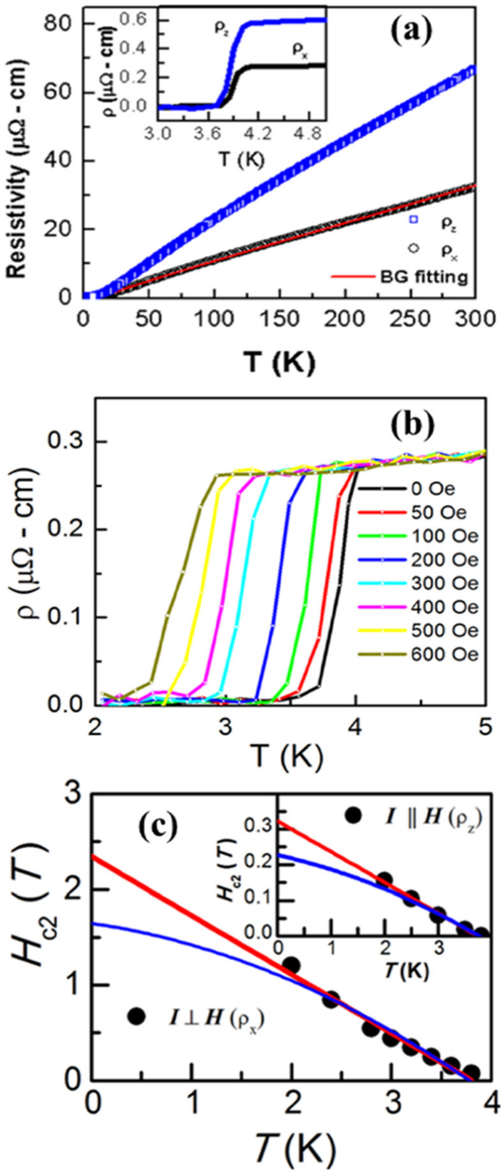

Figure 6. (a) ρ–T curves of a single crystal PbTaSe$_2$ for both in-plane (ρ_x) and out-of-plane (ρ_z). The inset figure shows the superconducting transition with vanishing ρ below $T = 3.8$ K for both crystallographic directions. (b) ρ_x–T curves at various H below 5 K for $I\perp H$. (c) The T dependence of the upper critical field H_{c2} for $I\perp H$ and $I/\!/H$ are plotted in the inset. The red solid lines indicate liner extrapolation to $T = 0$ K, and blue solid lilnes indicate the fitting of $H_{c2}(T)$ data to the Werthamer–Helfand–Hohenberg (WHH) theory.

The $\rho_x(T)$ ($5\,\text{K} \leqslant T \leqslant 300\,\text{K}$) data fit well with the BG model, as shown by the solid red curve in figure 6(a), which implies that the dominant scattering mechanism is a simple phonon–electron scattering above ~5 K. The obtained fitting parameters are residual resistivity $\rho_0 = 0.28$ $\mu\Omega$ cm, material dependent coefficient $A = 74.6$ $\mu\Omega$ cm, and a Debye temperature of $\theta_R = 96$ K. The in-plane $\rho_x(T)$ data measured under various magnetic fields (H) are depicted in figure 6(b). These data indicate that T_c decreases with increasing H and is suppressed to below ~2.2 K by 0.1 T, which is consistent to the $H_{c2} = 0.15$ T estimated from the $M(H)$ at 1.8 K as shown in inset of figure 5.

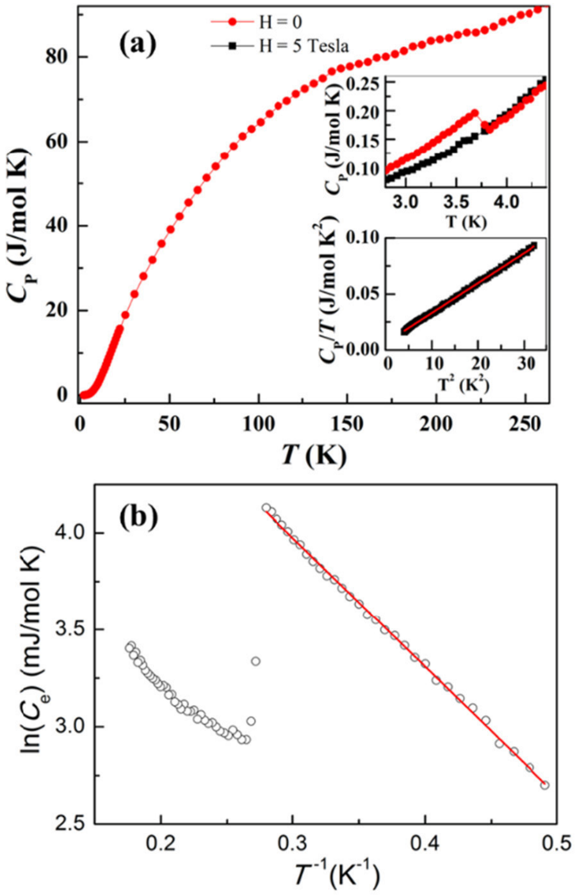

Figure 7. (a) Heat capacity C_p of PbTaSe$_2$ as a function of temperature T measured in zero magnetic field (main panel). The upper inset shows the low temperature regime under $H = 0$ and 5 T. The lower inset shows C_p/T versus T^2 in $H = 5$ T. The solid red line presents the linear fitting as described in the text. (b) The electronic specific heat in logarithmic scale is plotted as a function of $1/T$. The solid red line indicates the exponential function given by the BCS theory, see text for details.

The upper critical field H_{c2} is defined by the field at which $\rho = \rho_{\rm norm}$ $(H = 0)/2$ for $I \perp H$ and $I \parallel H$, as shown in figure 6(c). In general, the H_{c2} values are insensitive to the applied measurement method [28, 29]. The $H_{c2}(T)$ data is practically linear giving a slope of $dH_{c2}/dT = -0.77$ T K^{-1} for $I \perp H$, which is one order larger than that for $I \parallel H$ ($dH_{c2}/dT = -0.086$ T K^{-1}). However, based on the extrapolation of data down to $T = 0$, we found the $H_{c2}(0) = 0.323$ T for $I \parallel H$ which is almost one order smaller (2.34 T) than that for $I \perp H$. The observed strong anisotropy of resistivity and $H_{c2}(0)$ reflects the 2D transport network of a layered crystal structure with Van der Waals gap between layers, similar to that of NbSe$_2$ [25]. Nevertheless, the observe $H_{c2}(0)$ is much lower than the BCS theory expected Pauli limit of $\mu_0 H^{\rm Pauli}(0) = 1.86 T_c \sim 7$ T [30, 31], which could be due to the orbital and spin paramagnetic pair breaking.

For conventional weak-coupling BCS-type superconductors, the orbital limit of the H_{c2} can be described by the Werthamer–Helfand–Hohenberg (WHH) theory, H_{c2} approaches the value $H^{\rm orb}(0) = \alpha H'_{c2} T_c$, where $H'_{c2} = [dH'_{c2}(T)/dT]_{H=0}$ and α is purity factor with a value between 0.73 (clean limit) and 0.693 (dirty limit) [32, 33]. According to the WHH theory, the $H^{\rm orb}(0)$ value of clean limit is around 1.71 T (0.24 T) and dirty limit is around 1.62 T (0.22 T) for $I \perp H$ ($I \parallel H$). However, the observed $H_{c2}(T)$ data do not fit the WHH theory curve well but follow a T-linear behavior even at lower temperatures. Such a deviation of $H_{c2}(T)$ from the WHH theory has also been reported in other non-centrosymmetric superconductors, such as CaIrSi$_3$ [34] and SrAuSi$_3$ [35].

Thermodynamic properties. The heat capacity $C_p(T)$ of PbTaSe$_2$ single crystal sample measured at $H = 0$ and $H = 5$ T are displayed in figure 7(a),with the inset showing an expanded view for $T < 5$ K. The value of C_p at 250 K is near 90 J mol^{-1} K^{-1}, which is close to the Dulong–Petit high-T limit of the lattice heat capacity $C_V = 3nR = 99.8$ J mol^{-1} K^{-1} within experimental error. The bulk nature of superconductivity in PbTaSe$_2$ is evidenced by a sharp jump of $C_p(T)$ curve near 2.8 K measured at $H = 0$ (inset of figure 7(a)). The critical temperature $T_c = 3.78$ K is taken as the midpoint of the $C_p(T)$ jump, which agrees fairly well with that deduced from both the magnetic susceptibility (figure 5) and resistivity (figure 6) measurements. The superconducting state is completely suppressed by external applied magnetic field of 5 T, as expected when it is higher than the H_{c2} (see the upper inset of figure 7(a)). The $C_p(T)$ data is fitted using $C_p(T) = \gamma T + \beta T^3$ and the plot of $C_p(T)/T$ versus T^2 linear fit (lower inset of figure 7(a)) yields the electronic specific heat coefficient (Sommerfeld coefficient) of $\gamma = 5.96$ mJ mol^{-1} K^{-2} and phonon specific heat coefficient of $\beta = 2.69$ mJ mol^{-1} K^{-4}. Debye temperature $\Theta_D = 144$ K can be derived from β using the relationship of $\Theta_D = (12\pi^4 Rn/5\beta)^{1/3}$, where R is the molar gas constant and $n = 4$ is the number of atoms per formula unit. The value of Debye temperature Θ_D is higher than that of $\Theta_R = 96$ K estimated from the $\rho(T)$ data under the BG model, which has been suggested coming from the different assumptions of the Debye and BG models [35].

We find the derived ratio of $\Delta C_p/\gamma T_c = 1.46$ is close to the 1.43 given by the BCS theory for weakly coupled superconductors [9]. In the superconducting state, electronic specific heat ($C_e(T) = C_p(T) - \beta T^3$) follows a single BCS gap like $C_e(T) = A\gamma T_c \exp(-\Delta_0/k_B T)$ in the temperature range between 2 K and 3.7 K. Figure 7(b) shows the plot of $\ln C_e(T)$ versus $1/T$ with the fitted exponential function in solid line. The fitting parameters are $A = 17.6$ and energy gap $\Delta_0/k_B = 6.69$ K. The obtained energy gap is comparable to the limit of $1.76 k_B T_c$ of weakly coupled BCS superconductors [9]. In order to get some information on the strength of the electron–phonon coupling, we estimate the average electron–phonon coupling constant $\lambda_{\rm el-ph}$ using McMillan's theory [36]

$$\lambda_{\rm el-ph} = \frac{1.04 + \mu^* \ln(\Theta_D/1.45\, T_c)}{(1 - 0.62\mu^*)\ln(\Theta_D/1.45\, T_c) - 1.04},$$

where μ^* is the Coulomb repulsive screened parameter, usually assumed to be between 0.1 and 0.15 [36, 37]. Substituting $T_c = 3.73$ K, $\Theta_D = 144$ K, and $\mu^* = 0.13$ into above equation yields $\lambda_{\rm el-ph} = 0.74$, which is suggestive of a moderate electron–phonon coupling in PbTaSe$_2$. All of the extracted parameters shown above, including the superconducting anisotropy, the value of the specific heat jump $\Delta C_p/\gamma T_\mathrm{c}$ at T_c, the superconducting energy gap Δ_0/k_B, and the electron–phonon coupling λ_ep support that $\mathrm{PbTaSe_2}$ can be categorized as a weakly coupled superconductor.

Conclusions

A high-quality single crystal of hexagonal $\mathrm{PbTaSe_2}$ (space group $P\bar{6}m2$) was synthesized for the first time using a chemical vapor transport technique. The bulk superconductivity of $T_\mathrm{c} = 3.83 \pm 0.02\,\mathrm{K}$ is confirmed with electrical resistivity $\rho(T)$, magnetic susceptibility $\chi(T)$, and heat capacity $C(T)$ measurements. The parameters of electron–phonon coupling λ_ep, energy gap Δ_0/k_B, and the specific heat jump $\Delta C/\gamma T_\mathrm{c}$ at T_c imply that $\mathrm{PbTaSe_2}$ can be ascribed to a weakly coupled superconductor. Electronic band structure calculations show a complex Fermi surface and a moderately high DOS at the Fermi level.

Acknowledgment

RS and FCC acknowledge the support provided by the Academia Sinica research program on Nanoscience and Nanotechnology under project number NM004. FCC acknowledges support from Ministry of Science and Technology in Taiwan under project number MOST-102-2119-M-002-004. We thank Nanoscience and Technology thematic tesearch program of Academia Sinica, Taiwan.

References

[1] Bauer E *et al* 2004 *Phys. Rev. Lett.* **92** 027003
[2] Bauer E and Sigrist M (ed) 2012 *Non-Centrosymmetric Superconductors: Lecture Notes in Physics* vol 847 (Berlin: Springer)
[3] Butch N P, Syers P, Kirshenbaum K, Hope A P and Paglione J 2011 *Phys. Rev.* B **84** 220504
[4] Frigeri P A, Agterberg D F, Koga A and Sigrist M 2004 *Phys. Rev. Lett.* **92** 097001
[5] Gorkov L P and Rashba E I 2001 *Phys. Rev. Lett.* **87** 037004
[6] Kimura N, Ito K, Saitoh K, Umeda Y, Aoki H and Terashima T 2005 *Phys. Rev. Lett.* **95** 247004
[7] Akazawa T, Hidaka H, Fujiwara T, Kobayashi T C, Yamamoto E, Haga Y, Settai R and Onuki Y 2005 *J. Phys.: Condens. Matter* **16** L29
[8] Bauer E *et al* 2009 *Phys. Rev.* B **80** 064504
[9] Bardeen J, Cooper L N and Schrieffer J R 1957 *Phys. Rev.* **108** 1175
[10] Bauer E *et al* 2010 *Phys. Rev.* B **82** 064511
[11] Togano K, Badica P, Nakamori Y, Orimo S, Takeya H and Hirata K 2004 *Phys. Rev. Lett.* **93** 247004
[12] Badica P, Kondo T and Togano K 2005 *J. Phys. Soc. Japan* **74** 1014
[13] Ali M N, Gibson Q, Klimczuk T and Cava R J 2014 *Phys. Rev.* B **89** 020505
[14] Eppinga R and Wiegers G 1980 *Physica* B + C **99** 121
[15] Kresse G and Furthmller J 1996 *Comput. Mater. Sci.* **6** 15
[16] Chang T R *et al* 2016 *Phys. Rev.* B **93** 245130
[17] Yu R, Weng H, Fang Z, Dai X and Hu X 2015 *Phys. Rev. Lett.* **115** 036807
[18] Kim Y, Wieder B J, Kane C L and Rappe A M 2015 *Phys. Rev. Lett.* **115** 036806
[19] Xie L S, Schoop L M, Seibel E M, Gibson Q D, Xie W and Cava R J 2015 *APL Mater.* **3** 083602
[20] Bian G *et al* 2016 *Nat. Commun.* **7** 10556
[21] Zhang X, Liu Q, Luo J-W, Freeman A J and Zunger A 2014 *Nat. Phys.* **10** 387
[22] Riley J M *et al* 2014 *Nat. Phys.* **10** 835
[23] Bertoni R *et al* 2016 arXiv:1606.03218 (https://arxiv.org/ftp/arxiv/papers/1606/1606.03218.pdf)
[24] Mazaki H, Yamamoto K and Yasouka H 1991 *Magnetic Susceptibility of Superconductors and Other Spin Systems* ed R A Hein *et al* (London: Plenum) p 333
[25] Scheidt E W, Herzinge M and Fischer A 2015 *J. Phys.: Condens. Matter* **27** 155701
[26] Tanatar M A, Ni N, Samolyuk G D, Bud'ko S L, Canfield P C and Prozorov R 2009 *Phys. Rev.* B **79** 134528
[27] Blatt F J 1968 *Physics of Electronic Conduction in Solids* (New York: McGraw-Hill)
[28] Isobe M, Arai M and Shirakawa N 2016 *Phys. Rev.* B **93** 054519
[29] Lyard L *et al* 2002 *Phys. Rev.* B **66** R180502
[30] Chandrasekhar B S 1962 *Appl. Phys. Lett.* **1** 7
[31] Clogston A M 1962 *Phys. Rev. Lett.* **9** 266
[32] Helfand E and Werthamer N R 1966 *Phys. Rev.* **147** 288
[33] Werthamer N R, Helfand E and Hohenberg P C 1966 *Phys. Rev.* **147** 295
[34] Eguchi G, Peets D C, Kriener M, Maeno Y, Nishibori E, Kumazawa Y, Banno K, Maki S and Sawa H 2011 *Phys. Rev.* B **83** 024512
[35] Goetsch R J, Anand V K, Pandey A and Johnston D C 2012 *Phys. Rev.* B **85** 054517
[36] McMillan W L 1968 *Phys. Rev.* **167** 331
[37] Morel P and Anderson P W 1962 *Phys. Rev.* **125** 1263